

Local current injection into mesoscopic superconductors for the manipulation of quantum states

M. V. Milosevic,¹ A. Kanda,² S. Hatsumi,² F. M. Peeters,¹ and Y. Otuka²

¹Department Fysica, Universiteit Antwerpen, Groenenborgerlaan 171, B-2020 Antwerpen, Belgium

²Institute of Physics and TMS, University of Tsukuba, Tennodai, Tsukuba, Ibaraki 305-8571, Japan

(Dated: February 22, 2024)

We perform strategic current injection in a small mesoscopic superconductor and control the (non)equilibrium quantum states in an applied homogeneous magnetic field. In doing so, we realize a current-driven splitting of multi-quanta vortices, current-induced transitions between states with different angular momenta, and current-controlled switching between otherwise degenerate quantum states. These fundamental phenomena form the basis for discussed electronic and logic applications, and are confirmed in both theoretical simulations and multiple-small-tunnel-junction transport measurements.

PACS numbers: 73.23.-b, 74.78.Na, 85.25.Hv

Preparation and manipulation of discrete quantum states are crucial for applications of quantum physics in nanoscale electronics, particularly switching devices and memories. The needed quantum states with discrete conductance levels, and the external control of those, have been recently realized in solid electrolytes [1], graphene [2] (both voltage biased), light-driven molecular switches [3], and magnetic nanowires tuned by magnetic field [4]. With a similar goal, the current-driven processes started to attract immense attention since the demonstration that the magnetization state of a nanomagnet can be influenced directly by electrical current [5]. The key convenience is that locally applied current enables switching of individual submicron elements even in integrated electronic circuits.

The latest example of the fundamental role of current injection in low-dimensional physics is the achieved electric flipping of the magnetic vortex core [6], without change in the vortex chirality. Vortices, rotational flow of currents or matter with a characteristic cavity at the center, can be found in many subfields of quantum physics. In small magnetic elements, vortices owe their existence to shape anisotropy and demagnetizing fields [7]. In semiconducting quantum dots the rotation of electrons is induced by external magnetic field and vortices may form if this rotation is strong [8]. Spontaneous vortex nucleation has been recently observed even in exciton-polariton condensates [9], a composite boson system resembling superfluidity in Bose-Einstein condensates in which vortices are readily found [10]. Still, vortex matter is most intrinsic to superconductors in a magnetic field. It is particularly rich in samples comparable to the coherence length and/or penetration depth [11], where vortex states become strongly influenced by sample geometry [12]. Due to strong lateral confinement, vortices may even merge into a multi-quanta ("giant") vortex, otherwise unstable in an open geometry [13, 14]. Such vortices contain multiple phase change of 2π encircling the central cavity, and are also found in rotated

superfluids and in strongly confined quantum dots in a magnetic field [15].

Vortices not only represent a key feature of topologically confined quantum-mechanical systems but may also be of use for electronic device applications. It has been shown recently that each change in the core of magnetic vortices gives rise to a measurable electric signal [16]. Changes in vortex configurations in quantum dots intuitively lead to distinct features in electronic transport [17]. In superconductors, the quasiparticle excitations inside vortices [18] form coherent quantum-mechanical states that depend on the number and arrangement of trapped flux quanta. As a consequence, the sample conductance measured along the vortex lines is determined by the transparency of the given vortex configuration [19]. Therefore, with changing magnetic field and thanks to the consequent change in vortex states, different levels of conductance can be achieved and a quantum switch is realized. Up to date, varied magnetic field remains the only tool for control of the angular momentum of vortex states and their configuration. In this Letter, we present a new method for vortex manipulation in small superconductors – by strategically applied current. We demonstrate the first electronically triggered splitting of

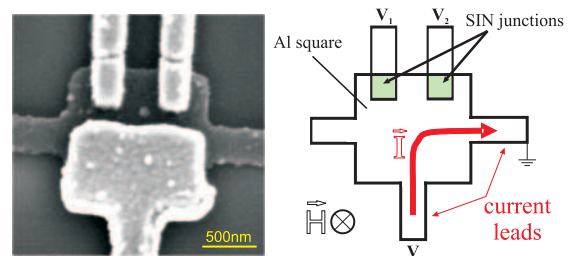


FIG. 1: SEM image of the sample – the mesoscopic superconducting square in a transport structure, with two tunnel junctions on top, as illustrated on the right (indicated directions of field and current are denoted positive). The details of fabrication can be found in Ref. [14].

the giant vortex as a fundamental novelty, controlled transitions between vortex states of different angular momentum for a given magnetic field (i.e. a current-driven quantum switch), as well as the manipulation of degenerate vortex equilibria from one to another, useful for logic applications.

Our sample is a $d = 40$ nm thick, $1:1:1:1$ μm^2 Al superconducting square designed for the multiple-small-tunnel-junction (MSTJ) measurement [14], in which two normal metal (Cu) leads (width $0.25 \mu\text{m}$) are connected to the top side of the sample through tunnel junctions (see Fig. 1). In addition, the square has three direct Al leads (width $0.3 \mu\text{m}$) centered at remaining sample sides, two of which are used for current (I) injection. The coherence length was estimated to $\xi(0) = 150-190$ nm, and the superconducting transition temperature T_c was 1.35 K. The magnetic field sweep rate was 3 mT/m in. In the MSTJ measurement, a small constant current (typically 1 nA) is applied to both junctions and the junction voltages, V_1 and V_2 , are measured simultaneously as a function of the magnetic field or the injected current I . An observed voltage reflects the local density of states and also the local supercurrent density underneath the junction, because the energy gap decreases with increasing supercurrent density. As a result, voltage jump corresponds to a transition between different vortex states. Furthermore, the comparison of voltage signals at two junctions indicates the symmetry of the circulating current, and thereby $V_1 \neq V_2$ points out the multi-vortex configuration, while $V_1 = V_2$ suggests a giant-vortex state.

To characterize the stationary and dynamic properties of the device, we solved numerically the time-dependent Ginzburg-Landau (TDGL) equation [20]

$$\frac{u}{\sqrt{1 + \frac{u^2}{2j^2}} \left(\frac{\partial}{\partial t} + i' + \frac{1}{2} \frac{\partial j^2}{\partial t} \right)} = (r - iA)^2 + (1 - j^2) \quad (1)$$

coupled with the equation for the electrostatic potential $\nabla' = \text{div}(\nabla - (r - iA))$. Here, the distance is measured in units of the coherence length ξ , t is scaled by its value in the absence of magnetic field ξ_0 , time by $\tau_{GL} = 2\hbar/\xi_0^2$, vector potential A by $\hbar/2e$, and the electrostatic potential by $\phi_0 = \hbar/2e\xi_0 = \hbar/2e_0d$, with τ_E being the inelastic electron-collision time (for Al samples, $\tau_E \approx 10$ ns gives $\tau_E \approx 10^3$). Parameter $u = 5.79$ is taken from Ref. [20]. Note that in Eq. (1) the screening of the magnetic field is neglected, as our sample is sufficiently thin to exhibit effective type-II behavior (therefore $A = \frac{1}{2}B(y; x; 0)$). The current leads (see Fig. 1) were simulated by imposing $\nabla' = j_i$, where j_i is the injected current density in units of $j_0 = c_0/8\xi^2$, $\nabla' = \nabla^2 d$. At the remainder of the sample edges, Neumann boundary condition was used ($j_n = 0$).

Fig. 2 shows the measured voltage and calculated Helmholtz free energy of the sample as a function of applied magnetic field ($F = \frac{1}{V} \int_V j^2 dV$, in units of

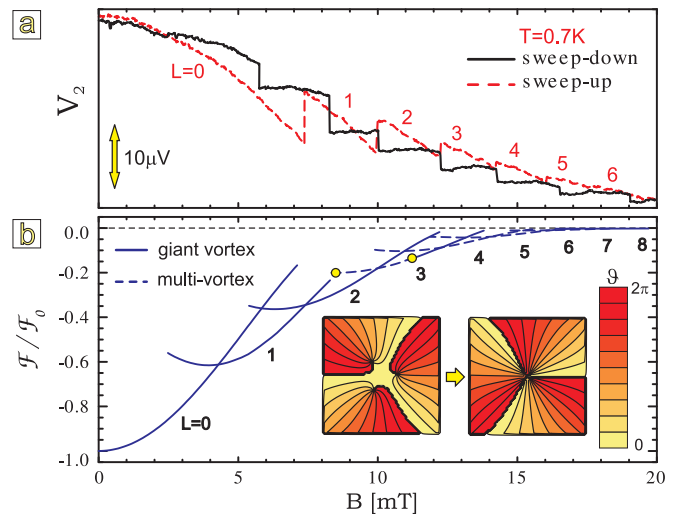


FIG. 2: Measured voltage (a) and calculated free energy (b) at $T = 0.7$ K. Insets show phase contour plots of the superconducting order parameter for $L = 3$ states (multi- and giant vortex) marked by open dots in free energy curves.

$F_0 = H_c^2/8$, where V is the sample volume). In Fig. 2 (b) different energy levels correspond to states with different angular momentum, i.e. vorticity L . Here taken $\xi(0) = 152$ nm and $T_c = 1.34$ K provided the best agreement with experimental vortex penetration/expulsion fields [see Fig. 2]. As already pointed out, some vortex states may exhibit ring-like configuration of individual vortices [13], i.e. a multi-vortex [dashed lines in Fig. 2 (b)], while in others all flux quanta coalesce into a single giant-vortex (solid lines). At higher temperatures, the characteristic lengthscales grow and effective competition favors giant-vortex states.

The distinction between the giant- and multi-vortex states in mesoscopic superconductors can also be made by monitoring of the vortex expulsion field B_e for a given state as a function of temperature, as detailed in Ref. [21] (decreasing $B_e(T)$ tendency is found for a multi-vortex vs. increasing $B_e(T)$ behavior for a giant-vortex state). Our measurements and calculations indicated that for e.g. $L = 3$ vortex state, the giant-vortex form is favorable above 0.9 K. In what follows, we investigate the influence of applied current on the shape of the vortex state. Following the scheme shown in Fig. 1, we applied weak dc current in the direction down-to-right, such that vortices experience Lorentzian-type of force ($\mathbf{F} = \mathbf{j} \times \mathbf{A}$) approximately towards top-left corner of the sample. Due to the spatial inhomogeneity of the force and the interaction with the sample boundaries, it can be energetically favorable for the giant-vortex to separate into individual ones and accommodate the imposed conditions. We achieved this giant-to-multi vortex splitting in both theory and experiment at temperatures above 0.95 K and this is the first such result in vortex physics. As shown

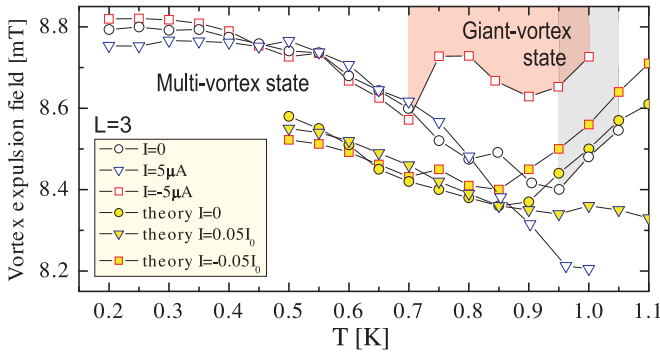


FIG. 3: Experimentally and theoretically obtained vortex expulsion field as a function of temperature for the $L = 3$ vortex state without and with applied current. Different behavior of the curves indicates multi- or giant- (shaded areas in experimental curves) vortex state.

in Fig. 3, for e.g. $T = 1.0$ K, we found a giant-vortex in the absence of applied current, but multi-vortex when even a weak current of $5 \text{ } \mu\text{A}$ was applied. In supplementary material [23], we also show the simulated dynamics of the giant-vortex splitting under applied drive at $T = 1$ K. Note however that in the case of opposite current ($I = -5 \text{ } \mu\text{A}$), the drive ‘drags’ vortices towards the bottom-right corner, where superconductivity is strong. This compresses the previously existing multivortex, and favors the giant-vortex state (see corresponding experimental curve in Fig. 3 for $0.7 < T < 0.95$ K). In addition, the vortex expulsion field is higher compared to $I = 0$ case, since the specific Lorentzian drive restricts access of vortices to the sides of the sample.

The above splitting of a giant-vortex by injected current is a non-equilibrium process, as giant- and multi-vortex realization of the same L -state cannot coexist. However, for a given multi-vortex state, there can be maximum n energetically degenerate vortex configurations with respect to sample boundaries. This fact forms a base for the fluxonic cellular automata [22], where e.g. two vortices in a square can occupy two alternative diagonal positions, forming states that can be labeled as logic ‘0’ and ‘1’. One of the essential problems in cellular automata is the successful preparation of inputs, i.e. the feasible manipulation of bits, and this can be realized by local current injection. In Fig. 4, we show the manipulation of the $L = 3$ multi-vortex state at $T = 0.7$ K. For sufficiently strong negative current, two vortices are attracted to the bottom-right corner rather than just one, which rotates the vortex structure by $\text{c.a. } 30^\circ$. In other words, the applied current enables the transition between otherwise degenerate states, and the switching is fully reversible. This is demonstrated in Fig. 4, where we realized multiple switching back and forth between two degenerate states by an alternating current. The rotation of the vortex configuration is verified by the alternating voltages measured at the two tunnel junctions.

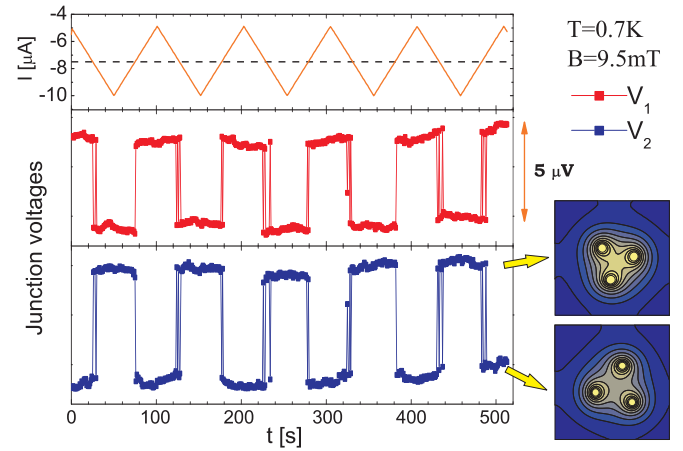


FIG. 4: Switching between degenerate vortex states (see insets) by alternating current ($|I| > 7.5 \text{ } \mu\text{A}$), demonstrated experimentally through measured voltages at junctions 1 and 2 (see Fig. 1).

Obviously, here reported phenomena are sensitive to the sample parameters, but crucially depend on the magnitude of the applied current. The larger current exerts larger force on vortices, which may expel some of them and/or help nucleate new ones in cases when, roughly speaking, local current on one of the sample edges exceeds the depairing current. The first scenario is particularly interesting at applied magnetic field which stabilizes several vortex states (see e.g. Fig. 2, for $B = 12$ mT). In such a case, one can induce controlled transitions between states of different vorticity by applying current of needed magnitude! We show this in Fig. 5(a), where one vortex is pulled out of the ground-state $L = 3$ giant-vortex (by $I < 0$), and double vortex ($L = 2$) remains stable after the current is switched off. Successful switching manifests as a peak of voltage V vs. time. If the same state was exposed to even larger current, vortices are sequentially expelled from the $L = 3$ state, but also new vortices appear at the opposite edge of the sample. Eventually, a ‘dynamic equilibrium’ is established (as shown in Fig. 5(b) and in supplementary animations [23]), exhibiting clear periodicity in the $V(t)$ signal linked to entry and exit of vortices. Latter oscillations of voltage are tunable by applied current, but in the present (A1) sample they are mostly in the GHz frequency range ($\tau_{GL} \approx 0.2$ ($L = T = T_c$) ps).

In Fig. 5(c) we show the experimental evidence for current-driven transitions between states of different angular momentum, at $T = 0.85$ K [24]. After decreasing magnetic field to $B = 11.2$ mT, the $L = 4$ to $L = 3$ transition was induced by applied current of $I = 15 \text{ } \mu\text{A}$, analogously to the scenario shown in Fig. 5(a). Voltage measured in further decreasing field shows that $L = 3$ state indeed remains stable. Therefore, our sample can

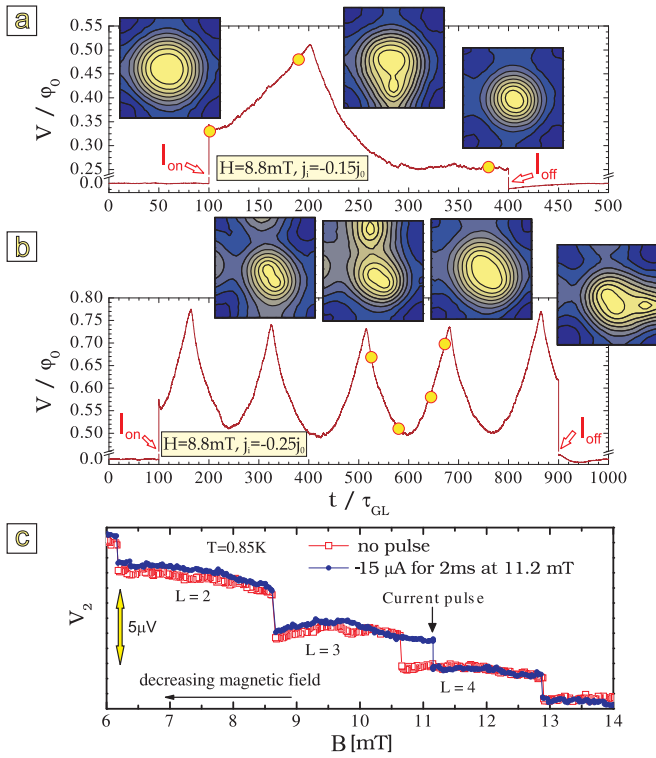


FIG. 5: Calculated voltage between current leads vs. time (at $T = 1.0$ K), for the case of (a) pullout of a vortex-quantum (transition from $L = 3$ to $L = 2$), and (b) active vortex penetration and expulsion, with average vorticity $L = 3$ (insets depict snapshots of the Cooper-pair density, see corresponding animations in [23]). (c) Experimentally measured voltage vs. decreasing applied field, prior and after the current-induced $L = 4 \rightarrow 3$ transition.

act as an excellent quantum switch, where applied current opens/closes the ballistic channel for quasiparticles through the vortex core (see Ref. [19]).

Latter $L = n \rightarrow n + 1$ transitions can be achieved for both polarities of the applied current, as one vortex can be either ‘pushed’ or ‘pulled’ out of the sample. In Fig. 6 we give the experimentally obtained values for the threshold current needed for enforced transitions between states with vorticity $0 < L \leq 4$ at $T = 0.85$ K, both for increasing and decreasing magnetic field. The typical values of minimal current needed for the switching were in the $|j| < 30$ A range for $T = 0.85$ K, and grew significantly with decreasing temperature (e.g. $|j| < 80$ A range for $T = 0.7$ K). Note that in some cases it becomes irrelevant if we perform vortex penetration or expulsion – e.g. at $B = 7$ mT, applied current of $I > 30$ A will provide $L = 1$ state, regardless of the initial vortex state ($L = 0$ or $L = 2$).

To summarize, we realized electronic control of the quantum states in a mesoscopic superconductor by strategic injection of dc current. Out of equilibrium, we performed the splitting of a giant, multi-quanta vortex into individual vortices. In equilibrium, we demonstrated

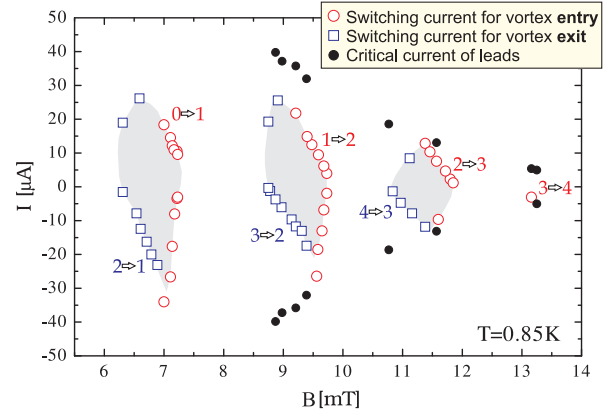


FIG. 6: Minimal switching current for states with $0 < L \leq 4$ (experiment done at 0.85 K), with distinction between the $L \rightarrow L - 1$ and $L \rightarrow L + 1$ processes (maximal current in experiment is limited by the critical current of the leads). The quantum switch was not operational in the shaded areas.

the current-induced transitions between states with different angular momenta, which also has a step-like effect on local ballistic conductance and is applicable as a quantum switch. Finally, switching between dual equilibria was also achieved, most useful for the fluxonic cellular automata. Local current injection therefore proves to be a powerful method for manipulation and preparation of quantum states on a submicron scale, and further work is needed to test the analogies in other quantum systems.

This work was supported by the Flemish Science Foundation (FWO-Vl), the Belgian Science Policy (IAP), JSPS/ESF-NES, and the Sumitomo and the Hitachi-Kurata Foundations.

-
- [1] K. Terabe et al., Nature (London) 433, 47 (2005).
 - [2] Y. Li et al., Nature Mater. 7, 966 (2008).
 - [3] M. DelValle et al., Nature Nanotech. 2, 176 (2007).
 - [4] V. K. Dugaev et al., Phys. Rev. Lett. 96, 047208 (2006).
 - [5] S. Krause et al., Science 317, 1537 (2007).
 - [6] K. Yamada et al., Nature Mater. 6, 269 (2007).
 - [7] R. P. Cowburn et al., Phys. Rev. Lett. 83, 1042 (1999).
 - [8] H. Saarikoski et al., Phys. Rev. Lett. 93, 116802 (2004).
 - [9] K. G. Lagoudakis et al., Nature Phys. 4, 706 (2008).
 - [10] M. R. Matthews et al., Phys. Rev. Lett. 83, 2498 (1999).
 - [11] A. K. Geim et al., Nature (London) 390, 259 (1997).
 - [12] B. J. Baelus and F. M. Peeters, Phys. Rev. B 65, 104515 (2002).
 - [13] V. A. Schweigert et al., Phys. Rev. Lett. 81, 2783 (1998).
 - [14] A. Kanda et al., Phys. Rev. Lett. 93, 257002 (2004).
 - [15] E. Rasanen et al., Phys. Rev. B 73, 235324 (2006).
 - [16] S. Prosdaveev and L. Bellaiche, Phys. Rev. Lett. 102, 097205 (2009).
 - [17] T. J. Gramila et al., Phys. Rev. Lett. 66, 1216 (1991).
 - [18] C. Caroli et al., Phys. Lett. 9, 307 (1964).
 - [19] A. S. Mel'nikov and V. M. Vinokur, Nature (London) 415, 60 (2002).

- [20] L. Kramer and R.J. Watts-Tobin, Phys. Rev. Lett. 40, 1041 (1978).
- [21] B.J. Baelus et al., Phys. Rev. B 71, 140502 (2005).
- [22] M.V. Milosevic et al., Appl. Phys. Lett. 91, 212501 (2007).
- [23] See EPAPS Document No. E-PRL-xxx-xxxxxx.
- [24] At $T > 0.9$ K, low measured voltage and low critical current of the superconducting leads hamper the precision of the measurement.